Buckling and Initial Postbuckling Behavior of Oval Cylindrical Shells Under Axial Compression[1]

J. W. HUTCHINSON
Assistant Professor,
Division of Engineering and Applied Physics,
Harvard University,
Cambridge, Mass.

Buckling and initial postbuckling behavior is determined for thin, elastic cylindrical shells of elliptical cross section. This study complements the buckling and advanced postbuckling calculations reported by Kempner and Chen on a similar class of shells. The initial postbuckling analysis indicates that, like compressed circular cylinders, the oval cylinders will be highly sensitive to small geometrical imperfections and may buckle at loads well below the predictions for the perfect shell. On the other hand, buckling will not necessarily result in complete collapse. A series of simple tests has been performed which provide qualitative verification of the major features of the theory.

Introduction

THE STUDY presented in this paper has been prompted by two interesting papers by Kempner and Chen [1, 2][2] on the buckling and postbuckling behavior of oval cylindrical shells under axial compression. In the second of these papers, the authors have presented results which indicate that an oval cylinder with sufficient eccentricity may be relatively insensitive to imperfections and may even be able to support loads significantly in excess of its classical buckling load. Of course, such behavior is in sharp departure from the extreme imperfection sensitivity of the circular cylinder under axial compression which under no circumstances can support loads above its classical buckling load.

The differences in the postbuckling behavior between the circular cylinder and an eccentric oval cylinder are prominently displayed in the load-deflection curves in Fig. 1. The curve for the perfect shell in Fig. 1(*b*) is a schematic reproduction from Kempner and Chen's paper [2]. The behavior in the early stages of buckling was not determined, but they tentatively conjectured it might follow the dotted segment of the curve in Fig. 1(*b*). If,

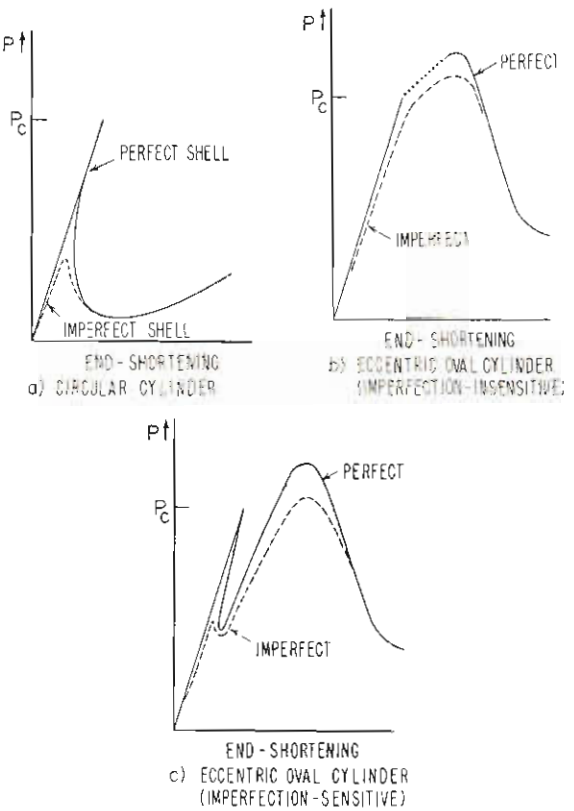

Fig. 1 Schematic load-end-shortening curves

[1] This work was supported in part by the National Aeronautics and Space Administration under Grant NsG-559, and by the Division of Engineering and Applied Physics, Harvard University.

[2] Nnmbers in brackets designate References at end of paper.

Contributed by the Applied Mechanics Division for publication (without presentation) in the JOURNAL OF APPLIED MECHANICS.

Discussion of this paper should be addressed to the Editorial Department, ASME, United Engineering Center, 345 East 47th Street, New York, N. Y. 10017, and will be accepted until April 15, 1968. Discussion received after the closing date will be returned. Manuscript received by ASME Applied Mechanics Division, January 25, 1967; final draft, May 11, 1967. Paper No. 67—APM-W.

Nomenclature

A = length of major axis of cross section
B = length of minor axis
b = initial postbuckling coefficient; see equation (13)
c = $[3(1-\nu^2)]^{1/2}$
E = Young's modulus
$\bar{F}$ = stress function
F = $q_0^2\bar{F}/(ER_0t^2)$, nondimensional stress function
$F^{(1)}, F^{(2)}$ = defined in equation (8)
$f^{(1)}, f_\alpha, f_\beta$ = defined in equations (16) and (22)
l = axial wavelength of buckle pattern
$\bar{N}_{xx}, \bar{N}_{xs}, \bar{N}_{ss}$ = membrane stresses
N_{xx}, N_{xs}, N_{ss} = $R_0/(Et^2)\cdot(\bar{N}_{xx}, \bar{N}_{xs}, \bar{N}_{ss})$
N_{xx}^0 = $\sigma^0R_0/(Et)$
P = applied axial load
P_C = classical buckling load
$P_{\max}$ = maximum support load prior to complete collapse
P_S = buckling load of imperfect structure (maximum support load in the initial postbuckling regime)
q_0 = $[12(1-\nu^2)]^{1/4}(R_0/t)^{1/2}$
R_B = radius of curvature at ends of minor axis
R_0 = (perimeter length $\div$ 2π), reference radius
R_S = local circumferential radius of curvature; see equations (2) and (5)

(Continued on next page)

in fact, this is true, the oval cylinder would be relatively insensitive to small imperfections as depicted by the dashed curve. An alternate possibility is suggested by the results of the present analysis and is shown in Fig. 1(c). According to this picture, initial buckling will be strongly influenced by imperfections but will not be catastrophic. Complete collapse occurs at a load above the primary buckling load.

The purpose of this paper is to present exact results for the initial postbuckling behavior and imperfection sensitivity of oval cylinders. The study is made within the context of Koiter's general theory of postbuckling behavior [3-5]. This analysis is specifically tailored to uncover the equilibrium behavior in the vicinity of the classical buckling load. This method is quite different from that employed by Kempner and Chen, who modified the scheme which has been used to obtain large-deflection behavior of circular cylinders. Their procedure is well suited for making large-deflection calculations but lacks accuracy and ease of application when applied to the initial postbuckling regime.

Mention can be made of several other studies which have aspects in common with the present work. Koiter [6] found that a narrow cylindrical panel under axial compression can have a stable or unstable postbuckling behavior depending on its width. Budiansky and Amazigo [7] have shown that buckling of cylindrical shells under hydrostatic pressure can be sensitive to imperfections in some instances and insensitive in others. The initial postbuckling behavior of toroidal shell segments under various loadings is strongly influenced by the relative magnitudes of the two principal curvatures [8].

Nonlinear Equations for Axial Buckling of Oval Shells

The points on the middle surface of a shell with an elliptical cross section satisfy

$$\left(\frac{\bar{y}}{A}\right)^2 + \left(\frac{\bar{z}}{B}\right)^2 = 1 \tag{1}$$

A circumferential coordinate $\bar{s}$ is introduced as shown in Fig. 2. The circumferential radius of curvature at any point on the ellipse is given by

$$R_s = \frac{A^2}{B}\left\{1 + \left[\left(\frac{B}{A}\right)^2 - 1\right]\left(\frac{\bar{y}}{A}\right)^2\right\}^{3/2} \tag{2}$$

For purposes of nondimensionalization, it is convenient to introduce a reference radius R_0 defined to be the radius of the circle with exactly the same perimeter as the ellipse; i.e.,

$$R_0 = \frac{\text{perimeter length}}{2\pi} = \frac{2A}{\pi}\int_0^{\pi/2}\left\{1 + \left[\left(\frac{B}{A}\right)^2 - 1\right]\sin^2\psi\right\}^{1/2} d\psi \tag{3}$$
$$= \frac{2A}{\pi}E(1, B/A)$$

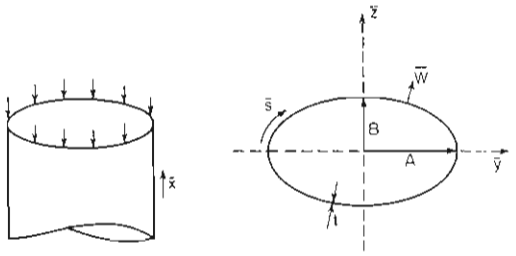

Fig. 2 Shell geometry

where E is the elliptic function of the first kind. The axial coordinate $\bar{x}$ and the circumferential coordinate $\bar{s}$ are nondimensionalized according to $x = \bar{x}q_0/R_0$ and $s = \bar{s}q_0/R_0$, where

$$q_0 = [12(1 - \nu^2)]^{1/4}(R_0/t)^{1/2} \tag{4}$$

and where t is the shell thickness, and ν is Poisson's ratio.

Kempner and Chen considered a different class of oval shells characterized by a circumferential radius of curvature

$$R_s = \frac{R_0}{1 - \xi \sin(2\bar{s}/R_0)} \tag{5}$$

where ξ, the "eccentricity parameter," gives rise to a circular cross section at one limit ($\xi = 0$) and at the other ($\xi = 1$) corresponds to an oval with $B/A \cong 0.485$ and an infinite radius of curvature at both ends of the minor axis [2]. Results for both cross sections will be presented.

The equations employed in the present analysis are the same as those used by Kempner and Chen. In appearance, they are identical to the nonlinear shallow shell equations and the Donnell-type equations for elastic deformation of thin shells. Application of these equations to the axial buckling of oval cylinders is justified because of the shallow buckling mode character of the buckling and initial postbuckling behavior. A more convincing argument can be given, however. On the basis of an ad hoc examination of the solutions, it was found that, in nearly all cases, Koiter's conditions for quasi-shallow shells [9] are met; and therefore, the solutions are completely accurate within the context of first-order nonlinear shell theory. Violations of the conditions occur at the ends of the major axis when the elliptical cylinders are very flat, but inaccuracy in the regions of high curvature has essentially no effect on the quantities governing overall shell behavior which have been calculated in this study.

The equations for an initially perfect shell are written here in a nondimensional form:

$$\nabla^4 W + \frac{1}{r(s)}F'' = 2c(F''W'' + F''W'' - 2F''W'') \tag{6}$$

$$\nabla^4 F - \frac{1}{r(s)}W'' = 2c(-W''W'' + W'^2) \tag{7}$$

The dimensional normal displacement $\bar{W}$ has been normalized by the shell thickness, $W = \bar{W}/t$, while the other quantities appearing in these equations are defined in the Nomenclature. Also, the abbreviations $(\ )^{\cdot} = (\ )_{,s}$, $(\ )' = (\ )_{,x}$, and $\nabla^4 = [(\ )''$

Nomenclature

$r = R_S/R_0$
$\bar{s}$ = circumferential coordinate
$s = \bar{s}q_0/R_0$, nondimensional circumferential coordinate
t = shell thickness
$\bar{W}$ = outward normal displacement
$W = \bar{W}/t$, nondimensional normal displacement
$W^0, W^{(1)}, W^{(2)}$ = defined in equation (8)
$w^{(1)}, w_\alpha, w_\beta$ = defined in equations (16) and (21)
$\bar{x}, \bar{y}, \bar{z}$ = Cartesian coordinates; see Fig. 2
$x = \bar{x}q_0/R_0$, nondimensional axial coordinate
δ = amplitude of buckling displacement; see equation (16)
$\bar{\delta}$ = amplitude of initial imperfection
θ = "flatness parameter"; see equation (34)
λ = defined in equation (16)
ν = Poisson's ratio
ξ = "eccentricity parameter"; see equation (5)
σ^0 = applied compressive stress
σ_C = classical buckling stress

$+ (\ )'']^2$ have been introduced. The nondimensional membrane stresses are related to the stress function F by $N_{xx} = F''$, $N_{x\theta} = -F'$, and $N_{\theta\theta} = F''$.

Buckling and Initial Postbuckling Analysis

The analysis which follows proceeds along the lines laid out by Koiter [3–5] for exploring the equilibrium behavior in the initial stages of buckling. A general development of this theory will not be given here; instead, just the essential steps of the calculation will be recorded. A number of results from the general theory have been taken directly from [10, 11], which contain a reworked version of Koiter's theory.

First, an analysis of the perfect shell is carried out. An asymptotic perturbation expansion for the normal deflection and stress function is developed about the primary state of uniform axial stress $-\sigma^0$. The amplitude δ of the deflection in the classical buckling mode, denoted by $W^{(1)}$, is the expansion variable, and W and F are written as

$$\begin{aligned} W &= W^{(0)} + (\delta/t)W^{(1)} + (\delta/t)^2W^{(2)} + \ldots \\ F &= -\tfrac{1}{2}N_{xx}{}^0s^2 + (\delta/t)F^{(1)} + (\delta/t)^2F^{(2)} + \ldots \end{aligned} \tag{8}$$

where $N_{xx}{}^0 = \sigma^0R_0/Et$ is the nondimensional prebuckling membrane stress, and $W^{(0)}$ is the prebuckling deflection. Implicit in the development of this expansion is the assumption, to be justified in what follows, that buckling is associated with deflection in a single classical buckling mode $W^{(1)}$. As is well known, this is not true for the circular cylinder under axial compression, which owes its highly unstable postbuckling behavior to nonlinear coupling between many simultaneous classical modes. For this reason, the present analysis does not encompass the limiting case of the circular cylinder.

A sequence of linear boundary-value problems is generated for the functions appearing in the foregoing expansion as described in [10, 11]. The first of the sequence is the eigenvalue problem for the classical buckling stress $c(N_{xx}{}^0)_C$ and $W^{(1)}$ and $F^{(1)}$:

$$\nabla^4W^{(1)} + \frac{1}{r}F^{(1)''} + 2c(N_{xx}{}^0)_CW^{(1)''} = 0 \tag{9}$$

$$\nabla^4F^{(1)} - \frac{1}{r}W^{(1)''} = 0 \tag{10}$$

Once the classical problem has been solved, it will also be necessary to solve the second boundary-value problem, whose field equations are

$$\begin{aligned} \nabla^4W^{(2)} + \frac{1}{r}F^{(2)''} + 2c(N_{xx}{}^0)_CW^{(2)''} \\ = 2c(F^{(1)}{}_{,s}W^{(1)''} + F^{(1)''}W^{(1)}{}_{,s} - 2F^{(1)'}W^{(1)'}) \end{aligned} \tag{11}$$

$$\nabla^4F^{(2)} - \frac{1}{r}W^{(2)''} = 2c(-W^{(1)''}W^{(1)}{}_{,ss} + W^{(1)'2}) \tag{12}$$

We ignore boundary conditions at the ends of the shell and thus, in effect, treat the case of an infinitely long cylinder. Solutions are sought which are periodic functions of the axial coordinate. The Euler mode is deliberately eliminated from consideration. Various possible solution symmetries or asymmetries are possible with respect to the major and minor axes. The circumferential boundary conditions for the first and second-order boundary-value problems appropriate to the different possibilities will be discussed in detail at a later point. Specification of the problems is completed by the additional requirement, not written here, that the inplane displacements of the shell middle surface be single-valued about any circumferential circuit of the shell.

Solutions to these two problems are used to calculate the equilibrium relation of applied axial load P to buckling deflection δ in the initial postbuckling regime.[3] This relation, which is necessarily symmetric in the buckling deflection for the present problem, can be written as

$$P/P_C = 1 + b\left(\frac{\delta}{t}\right)^2 + \ldots \tag{13}$$

An explicit expression for the postbuckling coefficient b is given in [10, 11] for a class of theories in which the present shell theory is included. In terms of the quantities of the first two boundary-value problems, the coefficient is

$$\begin{aligned} b = \Bigg\{ 2\int_S [F_{,xx}{}^{(1)}W_{,s}{}^{(1)}W_{,s}{}^{(2)} + F_{,ss}{}^{(1)}W_{,x}{}^{(1)}W_{,x}{}^{(2)} \\ - F_{,xs}{}^{(1)}(W_{,x}{}^{(1)}W_{,s}{}^{(2)} + W_{,s}{}^{(1)}W_{,x}{}^{(2)})]dS \\ + \int_S [F_{,xx}{}^{(2)}W_{,s}{}^{(1)2} + F_{,ss}{}^{(2)}W_{,x}{}^{(1)2} - 2F_{,xs}{}^{(2)}W_{,x}{}^{(1)}W_{,s}{}^{(1)}]dS \Bigg\} \\ \div \left\{ (N_{xx}{}^0)_C \int_S [W_{,x}{}^{(1)}]^2dS \right\} \end{aligned} \tag{14}$$

The character of the postbuckling behavior in the initial stages after buckling hinges on the sign and magnitude of b. If b is positive, the applied load P increases to values above the classical buckling load P_C with increasing buckling deflection. However, if b turns out to be negative, then the equilibrium load falls with increasing buckling deflection and the postbuckling behavior is unstable under dead loading. In such a case, the shell is imperfection sensitive and, in an actual test, small geometrical imperfections can greatly reduce the buckling load. Koiter has obtained an analytic relation between the static buckling load P_S and the imperfection amplitude $\bar{\delta}$ for the case in which the initial deviation of the middle surface is in the shape of the classical buckling mode. This expression, which is asymptotically valid for small $\bar{\delta}$, is

$$\left(1 - \frac{P_S}{P_C}\right)^{3/2} = \frac{3(3)^{1/2}}{2}(-b)^{1/2}\left|\frac{\bar{\delta}}{t}\right|\frac{P_S}{P_C} \tag{15}$$

The symmetric bifurcation behavior discussed in the previous paragraph is depicted in Fig. 3 along with plots of P_S/P_C versus

[3] By its definition in equation (8), δ is the amplitude of the maximum normal deflection since $W^{(1)}$ will be chosen such that its maximum value is unity.

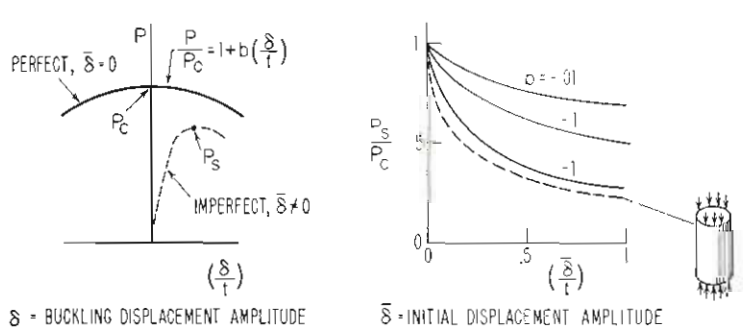

Fig. 3 Buckling of imperfection-sensitive shells

$\bar{\delta}/t$ for several values of b. Included in this figure is a curve, taken from Koiter [2], showing the effect of an axisymmetric imperfection on the buckling load of a circular cylinder under axial compression. Although the circular cylinder is not characterized by equations (13) and (15), this curve does provide a calibration for the postbuckling coefficient b for oval cylinders. It would be highly desirable to have relations between the buckling load and the imperfection obtained under less restrictive assumptions than equation (15) involving, perhaps, statistical measures of the imperfection. Such a characterization, however, is beyond the current state-of-the-art.

Solutions to the *classical buckling equations* (9) and (10) are sought in the form

$$W^{(1)} = w^{(1)}(s) \cos \lambda x \qquad F^{(1)} = f^{(1)}(s) \cos \lambda x \tag{16}$$

In this way, equations (9) and (10) are converted into a pair of coupled, ordinary differential equations with nonconstant coefficients:

$$w^{(1)\cdot\cdot\cdot\cdot} - 2\lambda^2 w^{(1)\cdot\cdot} + \lambda^4 w^{(1)} - \frac{\lambda^2}{r} f^{(1)} - 2\lambda^2 c(N_{xx}^0)_C w^{(1)} = 0 \tag{17}$$

$$f^{(1)\cdot\cdot\cdot\cdot} - 2\lambda^2 f^{(1)\cdot\cdot} + \lambda^4 f^{(1)} + \frac{\lambda^2}{r} w^{(1)} = 0 \tag{18}$$

The critical eigenvalue was found to be associated with a mode which was either symmetric with respect to both the major and minor axes (Mode I) or symmetric with respect to the minor axis and asymmetric with respect to the major axis (Mode II). Since a numerical method was used to solve equations (17) and (18), it was convenient to restrict consideration to a one-quarter segment of the circumference running from $s = 0$ to $s = \pi q_0/2$. The boundary condition at these points are

$$\left.\begin{aligned} w^{(1)\cdot} = w^{(1)\cdot\cdot\cdot} = f^{(1)\cdot} = f^{(1)\cdot\cdot\cdot} = 0 \\ s = 0,\ \pi q_0/2 \end{aligned}\right\} \text{Mode I} \tag{19}$$

and

$$\left.\begin{aligned} w^{(1)} = w^{(1)\cdot\cdot} = f^{(1)} = f^{(1)\cdot\cdot} = 0 \\ s = 0 \\ w^{(1)\cdot} = w^{(1)\cdot\cdot\cdot} = f^{(1)\cdot} = f^{(1)\cdot\cdot\cdot} = 0 \\ s = \pi q_0/2 \end{aligned}\right\} \text{Mode II} \tag{20}$$

Equations (11) and (12) for the *second-order boundary-value problem* also reduce to ordinary differential equations. The quadratic terms involving $W^{(1)}$ and $F^{(1)}$ on the right-hand sides of the equations give rise to nonhomogeneous terms which are either independent of the x-coordinate or vary as $\cos 2\lambda x$, where, of course, λ is predetermiued by the classieal analysis. Thus $W^{(2)}$ and $F^{(2)}$ are sought iu the separated form

$$W^{(2)} = c[w_\alpha(s) + w_\beta(s) \cos 2\lambda x] \tag{21}$$

$$F^{(2)} = c[f_\alpha(s) + f_\beta(s) \cos 2\lambda x] \tag{22}$$

and equations (11) and (12) reduce to

$$w_\alpha^{\cdot\cdot\cdot\cdot} = -\lambda^2 (f^{(1)} w^{(1)})^{\cdot\cdot} \tag{23}$$

$$f_\alpha^{\cdot\cdot\cdot\cdot} = {}^1/_2 \lambda^2 (w^{(1)2})^{\cdot\cdot} \tag{24}$$

and

$$w_\beta^{\cdot\cdot\cdot\cdot} - 8\lambda^2 w_\beta^{\cdot\cdot} + 16\lambda^4 w_\beta - 4\lambda^2 f_\beta/r - 8\lambda^2 c(N_{xx}^0)_C w_\beta = -\lambda^2 (f^{(1)\cdot} w^{(1)} + f^{(1)} w^{(1)\cdot} - 2 f^{(1)\cdot} w^{(1)\cdot}) \tag{25}$$

$$f_\beta^{\cdot\cdot\cdot\cdot} - 8\lambda^2 f_\beta^{\cdot\cdot} + 16\lambda^4 f_\beta + 4\lambda^2 w_\beta/r = \lambda^2 (w^{(1)\cdot} w^{(1)} - w^{(1)\cdot 2}) \tag{26}$$

The "loading terms" on the right-hand sides of equations (23)–(26) are quadratic in $w^{(1)}$ and $f^{(1)}$ and are symmetric with respect to the major and minor axes. The second-order contributions to the deflections and stresses will, therefore, be symmetric about this pair of axes. That is, for both Modes I and II,

$$\left.\begin{aligned} w_\alpha^{\cdot} = w_\alpha^{\cdot\cdot\cdot} = f_\alpha^{\cdot\cdot\cdot} = 0 \\ w_\beta^{\cdot} = w_\beta^{\cdot\cdot\cdot} = f_\beta^{\cdot} = f_\beta^{\cdot\cdot\cdot} = 0 \end{aligned}\right\} s = 0,\ \frac{\pi}{2} q_0 \tag{27, 28}$$

Equations (23) and (24) can be integrated by inspection such that the prescribed boundary conditions are satisfied. For our purposes, it is only necessary to determine $w_\alpha^{\cdot}$ and $f_\alpha^{\cdot\cdot}$; these are

$$w_\alpha^{\cdot} = -\lambda^2 \int_0^s f^{(1)} w^{(1)} ds + \lambda^2 (2s/\pi q_0) \int_0^{\pi q_0/2} f^{(1)} w^{(1)} ds \tag{29}$$

$$f_\alpha^{\cdot\cdot} = \frac{1}{2} \lambda^2 w^{(1)2} - (\lambda^2/\pi q_0) \int_0^{\pi q_0/2} w^{(1)2} ds \tag{30}$$

Note that the boundary conditions (27) are not sufficient to determine f_α but must be supplemented by the condition that f_α be single-valued, which insures that the circuit average of the membrane stress N_{zz} is the specified value N_{zz}^0. Also, the differential equation (23) and boundary conditions (27) yield a unique solution for w_α, except for an arbitrary constant which is determined by the further requirement that the circumferential tangential displacement he single-valued ahout any complete circuit of the shell. With this condition satisfied, it ean be shown that tangential displacements are single-valued up to and including terms of order $(\delta/t)^2$.

From this point, all ealculations were carried out numerically. The ordinary differential equations were finite-differenced and then solved using Potters' mcthod of Gaussian elimination [12]. The homogeneous differential equations (17) and (18) comprising the classical eigenvalue problem were solved for a number of values of λ to find for each value the lowest eigenvalue cN_{zz}^0. In a systematic way, the value of λ associated with the lowest eigenvalue of all $c(N_{zz}^0)_C$ was found along with the functions characterizing the classical buckling mode $w^{(1)}$ and $f^{(1)}$. Next, equations (25) and (26) were solved for w_β and f_β using the same Gaussian climination method. Finally, the postbuckling coefficient b was calculated using a standard method of numerical integration. A reduced expression for b can he obtained if the separated forms of equations (16), (21), and (22) are substituted in the general expression for b (14) and if, then, the integrations with respect to x are performed. This gives

$$\frac{b}{1-\nu^2} = \int_0^{\pi q_0/2} \left[-f^{(1)} w^{(1)\cdot} \left(w_\alpha^{\cdot} + \frac{1}{2} w_\beta^{\cdot} \right) + f^{(1)\cdot} w^{(1)} w_\beta - f^{(1)\cdot} w^{(1)} \left(w_\alpha^{\cdot} - \frac{1}{2} w_\beta^{\cdot} \right) - f^{(1)\cdot} w^{(1)\cdot} w_\beta - f_\beta w^{(1)\cdot 2} + \frac{1}{2} \left(f_\alpha^{\cdot\cdot} - \frac{1}{2} f_\beta^{\cdot\cdot} \right) w^{(1)2} - f_\beta^{\cdot} w^{(1)} w^{(1)\cdot} \right] ds + \frac{c(N_{zz}^0)_C}{6} \int_0^{\pi q_0/2} w^{(1)2} ds \tag{31}$$

Results of Buckling and Initial Postbuckling Analysis

Elliptical Cross Sections

Buckling initiates in the regiou of minimum curvature at the ends of the minor axis of the ellipse. If the shell is sufficiently thin, the classical stress approaches that of a circular cylinder whose curvature is the same as occurs locally at the ends of the minor axis of the oval shell; i.e.,

$$\sigma_C = [3(1-\nu^2)]^{-1/2} \frac{Et}{R_B}; \quad R_B = \frac{A^2}{B} \tag{32}$$

Plots of the classical huckling stress, normalized by the foregoing limiting value, are given in the upper half of Fig. 4. Over most

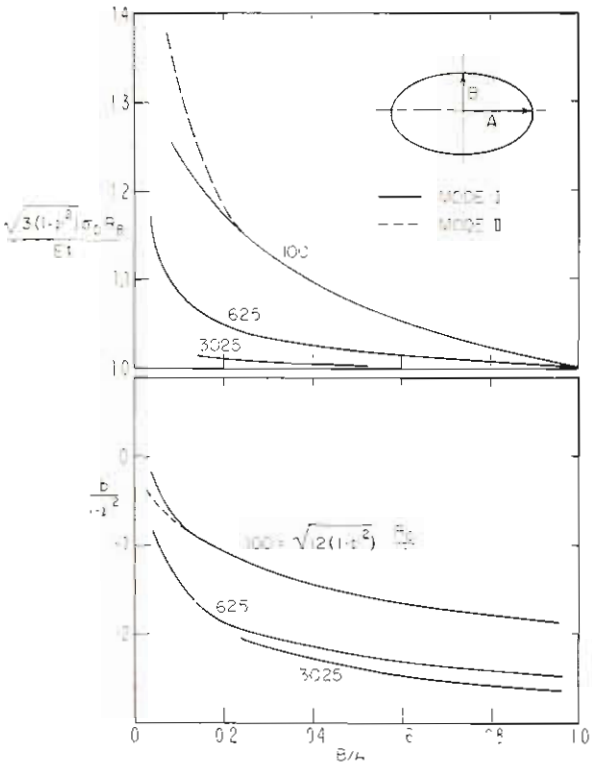

Fig. 4 Classical buckling and imperfection sensitivity of elliptical cylindrical shells under axial compression

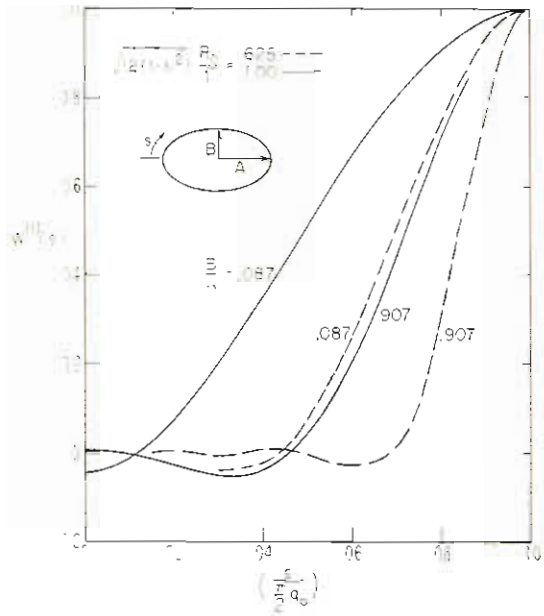

Fig. 5 Circumferential variation of buckling mode amplitude (Mode I)

of the range of B/A there is no appreciable difference between the critical stress associated with the doubly symmetric mode (Mode I) and the symmetric-asymmetric mode. However, in the lower range of B/A which has been plotted, the two cases diverge and Mode I is critical as shown in Fig. 4 for $q_0 = 10$.

Plots of the circumferential variation of the buckling mode are shown in Fig. 5. The curves shown were selected to display two features, found by Kempner and Chen as well, which characterize the classical buckling of oval cylinders. First, the region in which significant buckling takes place concentrates about the ends of the minor axis when the shells are very thin just as one would expect. The second feature is that the buckling mode of a near-circular oval ($B/A = 0.907$ is the case shown) is quite distinct in its radial deflection from any of the classical buckling modes of the circular cylinder. In the limit, this distinction vanishes. The axial wavelength of the buckling mode of the oval shell is roughly equal to the wavelength of the axisymmetric buckling mode of the corresponding circular cylinder of radius R_B

$$l = 2\pi[12(1 - \nu^2)]^{-1/4}(R_B t)^{1/2} \tag{33}$$

and approaches this value as q_0 becomes large.

The initial postbuckling coefficient b is displayed in the lower half of Fig. 4. Judging from our previous discussion and the curves in Fig. 3, the oval cylinders should be very imperfection sensitive for all but the most highly eccentric cross sections. Additional points in the range of very small B/A, where b does cross over to positive values, have also been obtained but will not be presented since this range is of little practical interest. On the other hand, it is of interest to relate this study to work on axially compressed narrow cylindrical panels by Koiter [6].

When B/A is very small, either side of the oval cylinder is much like a narrow curved panel and, if B/A is zero, it is essentially a flat plate. Koiter has shown that the transition from an unstable ($b < 0$) to a stable ($b > 0$) postbuckling behavior takes place when the panels are sufficiently close to the flat plate configuration. Similar behavior is expected to nearly flat elliptical cylinders. The "flatness paramcter" appropriate to the eccentric elliptical oval is

$$\theta = \frac{1}{2\pi}[12(1 - \nu^2)]^{1/4}\frac{2A}{(R_B t)^{1/2}} \tag{34}$$

Using boundary conditions which are somewhat different from those of either of Mode I or Mode II, Koiter found that the transition ($b = 0$) for the cylindrical panel occurred when $\theta = 0.64$. Our calculation gives $\theta \cong 0.8$ for Mode I and $\theta \cong 0.6$ for Mode II; for $q_0 = 10$, these values correspond to $B/A \cong 0.04$ and 0.02, respectively.

It can be shown that the analysis with the boundary conditions of Mode II for the limiting case $B/A = 0$ is exactly applicable to an infinitely long flat plate of width $2A$ which is simply supported along its two edges and compressed in the long direction. The initial postbuckling coefficient for the flat plate is $b = 3(1 - \nu^2)/8$, and the present numerical results for very small B/A did coincide with this value.

As mentioned previously, the analysis just outlined is not applicable to the circular cylindrical shell under axial compression because, for this problem, the assumption of a single classical buckling mode must be abandoned. Results have been obtained and plotted for near-circular cylinders with B/A as near unity as 0.96, and values of b in the neighborhood of -2 have been found as seen in Fig. 4. Judging from the asymptotic curves of buckling load versus imperfections in Fig. 3, it appears that near-circular cylinders are about as susceptible to imperfections as the circular cylinder. While this seems intuitively obvious, it is reassuring to see a qualitative verification of this similarity emerge from two quite different analyses.

Nonellipsoidal Oval Cross Sections

Although it seemed quite unlikely that the imperfection-sensitivity trends of the elliptical cylinders could be much different from those for the oval cylinders studied by Kempner and Chen, nevertheless, the calculations described were repeated for the nonellipsoidal cross sections. Results are plotted in Fig. 6 for $q_0 = 18.2$ corresponding to one of the values chosen by Kempner and Chen for their advanced postbuckling calculations. The classical buckling predictions agree completely with their calculations. The initial postbuckling predictions are at odds with their tentative curves for this region, which suggests a transition from imperfection sensitivity to insensitivity somewhere between $\xi = 0.5$ and 0.8 when, actually, the oval cylinders will be imperfection sensitive for all cross sections, including the limiting case $\xi = 1$. A careful examination of the present solution was made; and it

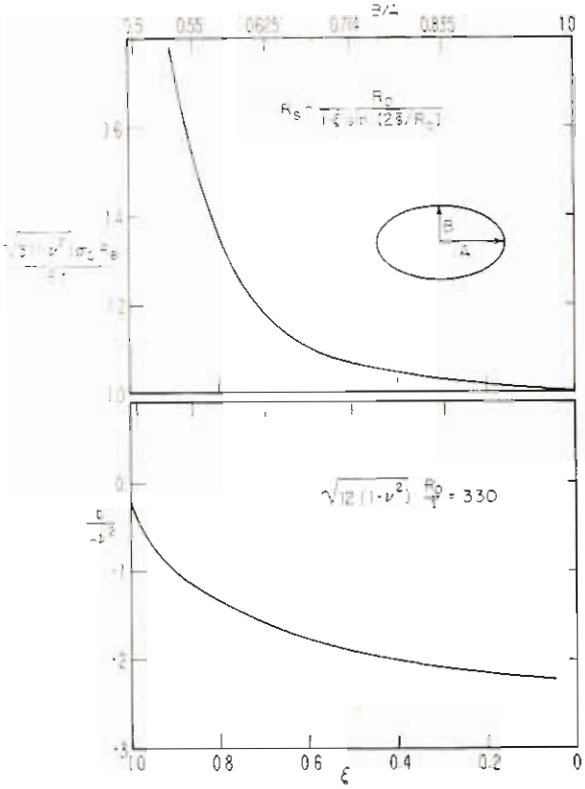

Fig. 6 Classical buckling and imperfection sensitivity of oval cylinders under axial compression (nonellipsoidal cross section)

became clear that, of all the second-order terms contributing to b, the x-independent terms, w_α^* and f_α^{**}, are by far the most important. The series representation used by Kempner and Chen could not yield accurate results in the initial postbuckling regime since the w_α^*-contribution of this series is identically zero.

Large-deflection calculations have acquired a reputation for being notoriously hard. The large-deflection load versus end-shortening relation for circular cylindrical shells has been recalculated many times; and, as Hoff, Madsen, and Mayers [13] have recently shown, this problem is still not completely resolved. Kempner and Chen's problem is even more difficult since one is almost forced to use trigonometric series representations, and these are not nearly so well suited for application to the oval cylinder as they are to the circular cylinder. Thus the exact initial postbuckling results complement the large-deflection calculations and enable one to construct a much clearer picture of the total buckling behavior.

It remains, then, to reconcile our initial postbuckling predictions with Kempner and Chen's prediction of a maximum support load, which is in excess of the classical buckling load when the oval cylinder is sufficiently eccentric, (the transition occurring for ξ somewhere between 0.5 and 0.8 for the nonelliptical ovals). This is accomplished in the manner hinted at in the Introduction and depicted schematically in Fig. 1(c).[4] A perfect shell would undergo snap buckling but not complete collapse when the classical buckling load P_C is attained. The buckling deflections would be confined mainly to the neighborhood at the ends of the minor axis. As the load is increased above P_C, buckles will spread to the regions of higher curvature until the entire shell collapses catastrophically. The imperfect shell will buckle at loads well below P_C but, again, will sustain greater loads before collapse occurs.

Tests of Elliptical Cylinders in Axial Compression

Ten specimens, two for each of five values of minor-major axis ratio ranging from $B/A = 1$ to 0.25, were subject to increasing amounts of axial compression under dead loading until they collapsed. The specimens were constructed of thin Mylar sheet which was formed around, and bonded to, wooden elliptical end pieces. The axial seam of overlapped sheet was made as narrow as possible and, in the case of the noncircular cylinders, was lined up with one of the ends of the major axis where it has the least effect on preliminary buckling. Each specimen was designed such that its classical buckling stress was a small fraction of the Mylar yield stress. This method of construction leads to residual stress in the unloaded shell; however, this stress should play far less of a degrading role than the initial waviness of the shell which is invariably present in shells fashioned in this way. According to the theoretical predictions, initial deviations on the order of the shell thickness should have a very observable effect on the buckling load.

Data on these specimens and the tests are listed in Table 1. Two circular cylinders were tested to provide a calibration of the overall quality of the construction. Both buckled at between one third and one fourth of the classical load and thus are more or less typical of the specimens of Weingarten, Morgan, and Seide [14] for $R/t = 800$. In accord with the discussion of the previous section, two "buckling loads" have been recorded: P_S is the load at which a distinct buckling pattern first emerges, and P_{max} is the collapse load. It was not possible to distinguish between P_S and P_{max} with the first six specimens, although even one of the circular cylinders developed a very slight, isolated dimple at loads below collapse. In contrast, specimens 7 and 8 underwent a fairly sharply defined preliminary buckling into a distinct pattern at P_S less than one half of P_C. The buckling amplitude was several times the shell thickness and grew in magnitude with increasing load until the shell collapsed. Preliminary buckling was less well defined in specimens 9 and 10, presumably because the shells were quite imperfect, and assignment of a value to P_S was somewhat arbitrary. Nevertheless, the maximum support load of specimen 9 was actually greater than the classical buckling load by about 25 percent.

[4] The exact load-end-shortening relation for the perfect shell, valid in the initial stages of buckling, is of the form

$$\frac{\epsilon}{\epsilon_C} = \frac{P}{P_C} + K\left(1 - \frac{P}{P_C}\right)$$

where ϵ_C is the value of the end-shortening ϵ at the critical load. The coefficient K has been calculated along with b; and, in all cases plotted for B/A greater than 0.1, ϵ/ϵ_C diminishes with decreasing P/P_C.

Table 1 Test Data

Specimen	B/A	R_0/A	A	B	l	P_C	b	$(P_S)_{exp}$	$(P_{max})_{exp}$
1	1	1.0	2.64	2.64	0.31	34 7	...	9.2	9.2
2	1	1.0	2.64	2.64	0.31	34.7	...	8.9	8.9
3	0.75	0.877	3.02	2.26	0.38	22.8	−2.3	6.5	6.5
4	0 75	0.877	3.02	2.26	0.38	22.8	−2.3	9.4	9.4
5	0.50	0.771	3.43	1.71	0.50	13.3	−2.1	5.1	5.1
6	0.50	0.771	3.43	1.71	0.50	13.3	−2.1	6.9	6.9
7	0.333	0.707	3.74	1.25	0.64	8 15	−1.9	2.7	4.9
8	0.333	0.707	3.74	1.25	0.64	8.15	−1.9	2.6	6.0
9	0.25	0.683	3.86	0.97	0.75	5.92	−1.8	2.5	7.6
10	0.25	0.683	3.86	0.97	0.75	5.92	−1.8	1.6	5.7

All loads in pounds, lengths in inches; $E = 10 \times 10^6$ psi; $t = 0.003$ in.; $q_0 = 53.7$; axial length of all specimens = 6 in.; ν is taken to be 1/3.

Clearly, conclusive experimental verification of the results and conjectures of the previous section cannot be based on these qualitative tests alone. Data on more nearly perfect shells are desirable. On the other hand, tbe test data are entirely consistent with the predictions of the initial postbuckling analysis as well as Kempner and Chen's predictions of collapse loads in excess of the classical bnckling load.

References

1 Kempner, J., and Chen, Y. N., "Large Deflections of an Axially Compressed Oval Cylindrical Shell," *Proceedings of the Eleventh International Congress of Applied Mechanics*, Munich, Springer-Verlag, Berlin, 1964, pp. 299–306.

2 Kempner, J., and Chen, Y. N., "Buckling and Postbuckling of an Axially Compressed Oval Cylindrical Shell," Polytechnic Institute of Brooklyn, PIBAL Report No. 917, Apr. 1966; presented at Seventh Anniversary Symposium on Shells to honor Lloyd H. Donnell.

3 Koiter, W. T., "On the Stability of Elastic Equilibrium" (in Dutch), thesis, Delft, Amsterdam, 1945.

4 Koiter, W. T., "Elastic Stability and Postbuckling Behavior," *Non-Linear Problems*, Langer, R. E., ed., University of Wisconsin Press, Madison, Wis., 1963.

5 Koiter, W. T., "General Equations of Elastic Stability for Thin Shells," presented at Seventh Anniversary Symposium on Shells to honor Lloyd H. Donnell, Apr. 1966.

6 Koiter, W. T., "Buckling and Postbuckling Behavior of a Cylindrical Panel Under Axial Compression," Report S. 476, National Aeronautical Research Institnte, Amsterdam, 1956.

7 Budiansky, B., and Amazigo, J. C., "Initial Postbuckling Behavior of Cylindrical Shells Under External Pressure," to be published.

8 Hutchinson, J. W., "Initial Postbuckling Behavior of Toroidal Shell Segments," *International Journal of Solids and Structures*, Vol. 3, No. 1, Jan. 1967, pp. 97–116.

9 Koiter, W. T., "On tbe Nonlinear Theory of Thin Elastic Shells," *Koninklijke Nederlandse Akademie van Wetenschappen, Proceedings, Series B*, Vol. 69, 1966, pp. 1–54.

10 Budiansky, B., and Hutchinson, J. W., "Dynamic Buckling of Imperfection-Sensitive Structures," *Proceedings of the Eleventh International Congress of Applied Mechanics*, Municb, Springer-Verlag, Berlin, 1964, pp. 636–651.

11 Budiansky, B., "Dynamic Bnckling of Elastic Structures: Criteria and Estimates," Harvard University, Report SM-7, Jan. 1966; also, *Proceedings of the International Conference on Dynamic Stability Structures*, Pergamon Press, New York, 1966.

12 Potters, M. L., "A Matrix Method for the Solution of a Second-Order Difference Equation in Two Variables," *Mathematisch Centrum*, Amsterdam, Report MR 19, 1955.

13 Hoff, N. J., Madsen, W. A., and Mayers, J., "Postbuekling Equilihrium of Axially Compressed Circular Cylindrical Shells," *Journal of the American Institute of Aeronautics and Astronautics*, Vol. 4, 1966, pp. 126–133.

14 Weingarten, V. I., Morgan, E. J., and Seide, P., "Elastic Stability of Thin-Walled Cylindrical and Conical Shells Under Axial Compression," *Journal of the American Institute of Aeronautics and Astronautics*, Vol. 3, 1965, pp. 500–506.

Reprinted from the March 1968
Journal of Applied Mechanics